TOWARD PROTON COMPUTED TOMOGRAPHY

H. F.-W. Sadrozinski, Senior Member IEEE
Santa Cruz Institute for Particle Physics and Center for Origins Studies, UC Santa Cruz, CA 95064

Abstract
We discuss progress on Proton Computed Tomography, which would be used in conjunction with or in place of X-ray Computed Tomography for imaging in proton therapy treatment planning and patient positioning.
We present the requirements for pCT, and present data analysis and Monte Carlo simulations from proton transmission studies.

I. Introduction

X-ray Computed Tomography (XCT) is by now the common way to image patients for diagnostics and treatment planning. The principle is simple: a cone beam from an X-ray tube traverses the patient and the transmitted beam is recorded in a fine-grained detector . The intensity of the X-rays depends on the differential attenuation of photons in the body, which is related to the atomic number Z of the tissue traversed. By rotating the device around the patient, stacked 2D maps of linear X-ray attenuation are generated, allowing a faithful reconstruction of the patient's anatomy. A large effort is devoted to ever faster and more sophisticated reconstruction algorithm, as the 2002 IEEE NSS/MIC program shows.

Proton radiation therapy is a precise form of radiation therapy. Avoidance of damage to critical normal tissues and prevention of geographical tumor misses require accurate knowledge of the dose delivered to the patient and verification of the correct patient position with respect to the proton beam. In existing proton treatment centers dose calculations are performed based on XCT and the patient is positioned with X-ray radiographs [1].

However, the use of XCT images for proton treatment planning ignores fundamental differences in physical interaction processes between photons and protons and is, therefore, potentially inaccurate. Further, X-ray radiographs mainly depict patients' skeletal structures and rarely show the tumor itself. Ideally, one would image the patient directly with protons, for example, by measuring their energy loss after traversing the patient [2]. This method has the potential to significantly improve the accuracy of proton radiation therapy treatment planning and the alignment of the target volume with the proton beam.

We recently have begun to investigate the feasibility of Proton Beam Computed Tomography (pCT) and Proton Transmission Radiography (PTR).

In this paper, we will briefly review the basic difference of X-ray and proton imaging and the benefits of protons in cancer treatment, followed by a historical review of pCT. We then review the requirements for pCT measurements. We describe our present experiment to explore the feasibility of pCT using a telescope of the silicon detectors, including a comparison with the results of Monte Carlo (MC) simulations, focusing on the usefulness of the angular information of the outgoing proton.

II. Interaction in Matter: X-Rays vs. Proton

Diagnostic and therapeutic X-rays interact with the imaged object mainly through the attenuation of photons, which in the energy range of several keV proceeds through Compton scattering. Thus the process is statistical in its form, and one measures the number of transmitted photons. After passing through a thickness *l*, the original number of photons is reduced exponentially to N(*l*):

$$N(l) = N_0 e^{-\mu \cdot l} \qquad (1)$$

where μ is the attenuation coefficient. Fig. 1a shows the attenuation coefficient [3] as a function of energy in the X-ray range of relevance for medical imaging (1-100 keV) for bone, water, muscle, and fat. The energy dependence is large, and with the exception of bone due to the higher atomic number of Ca, the values of μ are very close to that of water for the different types of tissue. This is the reason why X-ray images of tissue are of low contrast, while bone can be imaged very well. It should also be pointed out that in an uniform medium, the largest number of X-rays is absorbed at the entrance of the beams, so that the dose will be highest at the entrance, with an ever decreasing dose extending quite far into the medium. Thus a large volume of tissue is affected.

Protons with energies used in therapeutic applications (70 MeV – 250 MeV) lose energy mainly through inelastic collisions with atomic electrons as described by the Bethe-Bloch equation [4]. The energy loss ΔE is the integral over the specific energy loss along the track length *l*:

$$\Delta E = \int \frac{dE}{dx} dx \approx \sum \rho \frac{dE}{dx} \Delta l \qquad (2)$$

where dE/dx is the "stopping power", the specific energy loss in the density weighted track length $x = \rho * l$, with only a weak dependence on the material traversed, *i.e.* dE/dx ~ Z/A [5]. Figure 1b shows the proton stopping power for the same materials as in Fig. 1a [3]. The energy dependence is fairly strong in the interesting energy range, which will be exploited in our experiment, but the difference between different materials is small: due to the small difference in density: relative to water, bone has $\Delta\rho = 0.5$ g/cm^2, and the density difference between fat and muscle is about $\Delta\rho = 0.1$ g/cm^2. Thus proton CT is inherently

low-contrast. Equation 2 shows that measuring the energy loss essentially measures the density distribution in the traversed material.

Protons undergo multiple Coulomb scattering (MCS) while traversing the material. The projected scattering angle is energy and material dependent:

$$\theta_{MCS} \approx \frac{13.6MeV}{\beta \cdot p} z\sqrt{l / X_0} \qquad (3)$$

where z is the charge of the projectile (z = 1 for protons) and X_o is the radiation length [5]. For a 250 MeV proton traversing 20 cm of water, the multiple scattering angle is about $\Theta_{MCS} \approx 1^o$.

The basic interaction leaves the proton intact (unless it undergoes nuclear interaction), and the properties of individual particles, energy and exit angle, can be measured and the density distribution of the traversed material deduced. We have started a program to investigate the feasibility of pCT in support of proton therapy, described in Ref [6], with initial results given in Ref. [7].

III. Advantages of Proton Therapy and Tomography

The negative slope of the stopping power curves for proton shown in Fig. 1b has important consequence for the application of protons in therapy. While traversing the medium, the protons slow down, and thus their dE/dx increases until they stop. This is shown in Fig. 2 where the particle energy E and the energy loss ΔE in 1 mm path length are plotted vs. the proton path length in water. At the end of the (energy dependent) range, the protons loose a large amount of energy in a small distance and then stop. Thus protons have relatively low entrance dose with a plateau, a maximum dose at the depth corresponding to the range, and a rapid distal dose fall-off. For extended tumors, the energy of the proton beam is modulated to vary the range across the site of the tumor. As mentioned above, X-rays have a high entrance dose, moderate energy deposition at depth and contribute dose beyond the target area. There is an increasing numbers of low-energy proton accelerators dedicated to therapy [8]. Proton CT can directly measure the density distribution needed for range calculation, while. X-ray CT use in proton cancer therapy can lead to large uncertainties in range determination, as shown in Ref [9]: range uncertainties introduced by using XCT as compared to PTR measurements can reach more than 15 mm in certain locations in the head.

There is an expectation (hope?) that with pCT the required dose to the patient can be reduced.

IV. Milestones in Proton Computed Tomography

A. Historical Development

Interest in pCT started with the observation of in R. R. Wilson in 1946 [10] that the Bragg peak and defined range of mono-energetic hadrons could be used for precision treatment of cancer. Wilson's vision of using either existing HEP accelerators or dedicated medical hadron machines for cancer treatment has been pursued ever since [8].

The use of protons for imaging ("Tomography") was advocated by A. M. Cormack in 1963 [11], and in 1972, M. Goitein [12] elucidated the methods to acquire 2-D data and to reconstruct 3-D images, backing it up by simulations. A. M. Cormack and A. M. Koehler [13] showed in 1976, that pCT can detect extremely low-contrast features by imaging sugar solutions with a density difference of $\Delta\rho << 0.5$ % relative to water. The LANL group of K. M. Hanson et al. [14] showed in 1982 imaging of human tissue using a high precision range telescope. In their study they pointed out, that pCT has a dose advantage with respect to XCT when imaging tissue, which, as pointed out before, has inherently low-contrast in both methods. Recently the PSI group of U. Schneider, E. Pedroni et al. [15] has been very active in both calibrating CT values, and in developing a working pCT system. The BNL group [16] pointed out a potential dose advantage of pCT, i.e. reduced dose of Proton CT compared to X-Ray CT.

B. What is new in pCT

There are several factors, which have led to a renewed interest in pCT. One is the increased number of dedicated accelerator facilities with gantry beam delivery systems [8]. There is interest in academia with fairly recent PhD theses at PSI [17], [18] and Harvard Cyclotron [19], which investigate the usefulness of pCT. Another reason is the availability of high bandwidth detector systems for the detection of the protons which will reduce the required beam time. One option is using semiconductor detectors, which do not use consumables like gas, making the instrumentation less complicated and more compact. They allow high particle rate in excess of a few MHz, can be tiled from large-scale (6") wafers and are fine-grained (50-100's μm pitch). A third reason is a growing simulation effort , which uses modern Monte Carlo codes like GEANT4 with worldwide support. They allow to exploit the correlation between scattering angle and energy, and can be used in the entire proton imaging and treatment process, includes the optimization of the beam energy, design of the pCT instrumentation, data analysis and dose calculation and minimization.

V. Sensitivity Study

The consequences of the low contrast in pCT can be shown in a simple one-dimensional sensitivity study using the energy loss data tabulated by NIST [3]. We approximate tissue with a 20 cm deep water column of large sideways dimension, and imbed at the midpoint an inclusion layer of thickness l = 1 cm. The density ρ of the layer is varied from 1.0 to 1.1, 1.5 and 2.0 g/cm^3. The effect of the difference in energy loss on 250 MeV protons is shown in Fig.3. In Fig. 3a, the energy loss in 1mm

water is shown, showing the entrance plateau and the increased energy loss in the 1 long cm inclusion depending on the density selected. In Fig. 3b, the proton energy is plotted as a function of water depth for the four densities of the inclusion, showing only a slight dispersion in energy at the exit at 20 cm depth. Table1 shows the attributes of the exiting protons which could be measured as a function of the density, for different $x = \rho * l$. Again, the differences are very small: for a 10% density increase, the exit energy changes by 0.5 MeV, the range by 1mm, and the TOF in a 20 cm TOF system by 2ps. The energy straggling in 20 cm water is about 1 MeV, and the corresponding range straggling about 2mm, such that the energy difference in the low contrast case can only be determined statistically (see below).

VI. Requirements for pCT Measurements

The results in the last section indicate the importance of selecting an optimized measuring instrument to determine the proton energy to such accuracy that small density changes can be detected. Tracking of individual protons requires the following measurement on the protons:

- The location, before (?) and after the object, to few hundred μm
- The entrance (?) and exit angle to much better than the MCS angle $\theta_{MCS} \approx 1^{o}$.
- The average energy <E> to much better than a %.

Silicon strip detectors (SSD) afford position resolution of 50 μm or better, and the first two requirements can be met easily with a very compact SSD telescope arrangement. The most exacting requirement is the good energy (or range) measurement Here the energy determination can be improved with statistics, because the error on the average energy $\sigma_{<E>}$ decreases with an increased number N of protons measured:

$$\sigma_{<E>} = \frac{\sigma_E}{\sqrt{N}} \tag{4}$$

A practical limit to improving the energy determination is given by the requirement to minimize the dose to the patient. The dose D is defined as absorbed energy per mass, and thus only a function of the fluence N/A, where A is the area:

$$\mathrm{D} = \frac{\mathrm{N}}{\mathrm{A}} \cdot \frac{dE}{dx} \tag{5}$$

Inside the imaged object, one can define a small volume ("voxel"), which one wants to resolve. It has a linear dimension d with a density difference $\Delta\rho$ relative to the object. To achieve an energy measurement with 3 sigma significance passing through the voxel, one needs N protons, which will deposit a dose D_v. To set the scale, for a cubical voxel of size 1 mm, 10^5 protons of 200 MeV deposit a dose of D_v = 7 mGy (close the target dose for XCT). Thus there is a large number of photons which one can play with! Assuming a 2-D image, the number of different views is n = 20 cm / d, and the total dose is $D = n * D_v$. The dose for imaging the voxel will then depend on the energy resolution of the detector σ_E, the density difference $\Delta\rho$ and the voxel size d:

$$\mathrm{D} \sim \frac{{\sigma_E}^2}{\Delta^2 \rho \cdot d^5} \tag{6}$$

Thus for a fixed dose, the voxel size ("resolution") and the density difference ("contrast") can be traded off against each other. Independently, Eq. 6 indicates that one needs the best energy resolution, subject to energy straggling mentioned above. Thus an energy resolution of better than 1 % is required, with a dynamic range from about 50 MeV to 250 MeV. In Figure 4, the relationships between dose and the density difference are shown for several voxel sizes. The energy resolution (including energy straggling) is taken to be 2% for most cases. The dose penalty for using a detector of 20% resolution like a single silicon plane is also shown for a voxel size of 5 mm.

VII. Experimental pCT Study

Our approach in the preliminary PRT and PCT studies [6,7] is based on state-of-the-art silicon strip detectors (SSDs), which measure the energy and position of individual protons. The SSDs provide information about the position of the particle track from the strip-hit information, and about the particle's energy via the energy deposition measured in each detector. This system, described in greater detail in [20, 21], permits measurements of the proton position to about 50μm and determination of the energy of protons in the 20-300 MeV range. The proton energy is derived from the specific energy deposition in each SSD using the time over threshold (TOT) signal as described in [22, 23]. This is possible due to the relative steep energy dependence of the stopping power (Fig. 1b). Using the expected and experimentally confirmed TOT vs. energy curve, we find that the energy resolution σ_E / E below 40 MeV is on the order of 15 % and increases to about 25 % at 250 MeV. While this is not good enough for the final pCT system, it allowed us to gain valuable experience in data reconstruction and simulation.

The setup for our initial experiment, described in detail in Ref. [7], was installed on the research beam line of the medical proton synchrotron at Loma Linda University Medical Center [1]. A monochromatic 250 MeV proton beam was degraded by a 25.4 cm thick wax block to a mean energy of about 130 MeV. After a drift distance of 25 cm, the beam encountered the image object, a 5.0 cm long hollow aluminum cylinder, of outer diameter OD = 3.0 cm, and inner diameter ID = 0.68 cm. Behind the object, protons were individually detected by two silicon detector modules, each consisting of a pair of single-sided SSDs with

strips oriented at right angle to each other. These detectors, located immediately behind and 27cm downstream of the object, served to measure the spatial coordinates, *x* and *y*, and energy of the protons that either passed by or traversed the object. In addition, they allow to reconstruct the exit angle of the protons.

Proton transmission images were calculated for each SSD module by averaging the proton energy over a large number (~10^6) of individual events. The three-dimensional plot in Fig. 5 shows the spatial distribution of average energy in the upstream module with single strip resolution (pixel size approximately 0.2 x 0.2 mm^2). The image of the phantom projection is clearly seen in the spatial energy distribution. Note that the depth of the structure in Fig. 5 is directly proportional to the energy loss in the aluminum object and thus is proportional to the product of its length and density. Fig. 5 thus demonstrates the principle possibility of image formation based on the spatial measurement of proton energy loss behind the image object.

VIII. GEANT4 Simulations

To better understand the features of the proton transmission images presented in Section VII, we performed simulations with the Monte Carlo code GEANT4. The GEANT4 code has proved its ability to faithfully simulate the interaction of protons down to low energy [24]. Here, the code will be used to define cuts on the data to optimize spatial resolution and contrast of the proton images. Details of the simulations are given in Ref [25], which showed excellent agreement between data and simulated angular distributions. The angular spread for protons which traverse the pipe in its entirety is about 5^o, and for protons which miss the pipe completely about 1^o. The difference between the distributions is caused by the increased multiple Coulomb scattering in the pipe (see Eq. 3), an indication that the simulations can be used further to explore the usefulness of angular cuts. With the selected cut at 0.025 (about 1.5^o), protons with larger angular divergence are rejected, which eliminates about 50% of all protons passing through the object.

The result of this cut on the simulated energy profile in the *x*- and *y* silicon planes close to the object is shown in Fig. 6. The location of the profile corresponds to a slice across the center of the pipe in Fig. 5. The simulated energy profile (Fig. 6a) agrees well with the measured outline of the object (and with the measured energy profile, not shown here, within the limits of the calibration). The mean simulated energy of protons transmitted through the hole is about 10% lower than that for protons passing outside the object. Furthermore, in agreement with the measured energy profile, both the inner and outer walls of the pipe appear fuzzy in the energy profile.

These image features can be explained by "migration" of protons from the object into the surrounding space due to multiple Coulomb scattering. This assumption is supported by the distribution of the energy spread, shown in Fig. 6b, which is larger at the interfaces between the object and the surrounding air, indicating a mixture of protons with and without energy loss in this region. Protons with lower energies entered the object trough the front surface and exited through the sides. These protons "scattering out" also cause the fuzzy edge profile.

Applying now the angular cut removes most of the migrating protons and sharpens the image considerably. In Fig. 6a, the open symbols correspond to the energy profile with angular cut applied. The edges become sharp, with a transition from Al to air almost within a bin of 400 μm. In addition the central hole fills in. The energy RMS plot Fig. 6b (in red: without angular cut, in green with angular cut) indicates that the RMS is increased just in one bin, otherwise it is constant across the region of Al pipe and air, respectively. Thus there is strong evidence that the resolution of the pCT image can be improved by cuts on the exit angle.

IX. Conclusions

The renewed interest in imaging with Proton Computed Tomography is based on several factors: many new accelerators for proton therapy, academic interest, new simulation codes and the use of new detector systems.

Our exploratory pCT show that imaging with protons based on energy-loss measurement in silicon is possible, but most likely not good enough for an optimized system, which has to minimize the dose to the patient. The simulations with the GEANT4 program describe the features of the images well, e.g., the influence of multiple scattering and proton migration on the energy and position resolution. We have shown that it is possible to mediate the effects of multiple scattering by measuring the exit angles of individual protons with the silicon telescope and applying appropriate cuts.

.

X. Acknowledgments

I acknowledge with great pleasure discussions with Reinhard Schulte (LLUMC), David Williams, Brian Keeney and Leah Johnson (all at UC Santa Cruz), and Mara Bruzzi (Univ. of Firenze). I would like to thank the organizers of the 2002 NSS/MIC Symposium for a very stimulating meeting. This work was supported by Calspace.

XI. References

[1] J.M. Slater, J.O. Archambeau, D.W. Miller, M.I. Notarus, W. Preston, J.D. Slater, "The proton treatment center at Loma Linda University Medical Center: rationale for and description of its development", Int J Radiat Oncol Biol Phys.**22**:383-89, 1992.

[2] U. Schneider, E. Pedroni, "Proton radiography as a tool for quality control in proton therapy", Med Phys.**22**:353-63, 1995.

[3] National Institute for Standards and Technology, PSTAR database, http://physics.nist.gov/PhysRefData/Star/Text/PSTAR.html

[4] H.Bichsel, "Passage of charged particles through matter", Amer. Inst. of Physics Handbook, McGraw Hill, 8-142 – 8-189, 1972.

[5] D.E. Groom ed., "Review of Particle Physics," *Eur. Phys. J,* vol. C15, pp.1-878, 2000.

[6] H. F-W. Sadrozinski *et al*, "Issues in Proton CT", VERTEX2002 Kona, HI, Nov. 2002, SCIPP 02/34.

[7] L. R. Johnson *et al*. "Initial Studies from on Proton CT using a Silicon Strip detector Telescope", RESMDD02, Florence, Italy, July 2002, SCIPP 02/32.
[8] S. Peggs, "Proton Therapy Accelerators", 2002 IEEE NSS/MIC in Norfolk, VA, Nov. 2002.
[9] U. Schneidert, E. Pedroni and A. Lomax," The calibration of CT Hounsfield units for radiotherapy treatment planning", Phys. Med. BioI. 41:111-124,1996.
[10] R.R. Wilson "Radiological use of fast protons," Radiology 47, 487, 1946.
[11] A. M. Cormack , "Nobel lecture", http://www.nobel.se/medicine/laureates/1979/cormack-lecture.pdf
[12] M. Goitein, "Three-Dimensional Density Reconstruction from a Series of Two-Dimensional Projections", Nucl. Inst. Meth., vol **101**, pp. 509-518, 1972.
[13] A. M. Cormack and A. M. Koehler, "Quantitative proton tomography" Phys. Med. Biol. **2**1:560-69, 1976.
[14] K M Hanson, J N Bradbury, R A Koeppe, R JMacek, D R Machen, R Morgado, et al., "Proton Computed Tomography with human specimens" , Phys. Med. Biol. 27:25-36, 1982.
[15] Uwe Schneider and Alexander Tourovsky, "Range-Uncertainty Imaging for Obtaining Dose Perturbations in Proton Therapy", IEEE Trans Nuc Sci Vol 45 No 5, p. 2309 (October 1998)
[16] T. J. Satogata T. Satogata, T. Bacarian, S. Peggs, A.G. Ruggiero, and F.A. Dilmanian, "Reduced Dose of Proton CT Compared to X-Ray CT in Tissue-Density Variation Sensitivity", (Poster M10-204) 2002 IEEE NSS/MIC in Norfolk, VA, Nov. 2002.
[17] U. Schneider, "Proton Radiography : A tool for quality control in proton therapy", PhD Thesis,, ETH Zurich, 1994
[18] P. Pemler, "Entwicklung, Bau und Test eines Detektorsystems für in vivo Protonenradiographie FROG", PhD Thesis, LMU Munich, 1997.
[19] P. Zygmanski, " ", PhD Thesis
[20] B. Keeney, V. Bashkirov, R.P. Johnson, W. Kroeger, H. Ohyama, *et al*., "A silicon telescope for applications in nanodosimetry", accepted for publication in IEEE Trans. Nucl. Science, **49**, 2002.
[21] B. Keeney, "A silicon telescope for applications in nanodosimetry", UC Santa Cruz Physics Senior thesis 2002, SCIPP 02/16.
[22] E. do Couto e Silva, G. Godfrey, P. Anthony, R. Arnold, H. Arrighi, *et al*, "Results from the beam test of the engineering model of the GLAST LAT," Nucl. Inst. Meth., vol. **474**/1, pp. 19-37, 2001.
[23] R. P. Johnson, P. Poplevin, H. F.-W. Sadrozinski, and E. Spencer, "An amplifier-discriminator chip for the GLAST silicon-strip tracker," IEEE Trans. Nucl. Sci., vol. **45**, pp. 927-932, 1998.
[24] GEANT4 Workshop at SLAC Feb 18-22, 2002, http://geant4.slac.stanford.edu/UsersWorkshop/.
[25] L. R. Johnson *et al*. "Monte Carlo studies of proton CT using a silicon strip detector telescope", 2002 IEEE NSS/MIC in Norfolk, VA, Nov. 2002, SCIPP 02/35.

TABLE 1 VALUE OF PROTON PARAMETERS AFTER 20CM OF WATER AND 1CM INCLUSION OF DENSITY ρ

$\rho * l$ [g/cm^2]	**Energy [MeV]**	**Range [cm]**	**TOF [ps]**
1.0	164.1	38.2	1309
1.1	163.6	38.1	1311
1.5	161.5	37.7	1317
2.0	158.9	37.2	1325

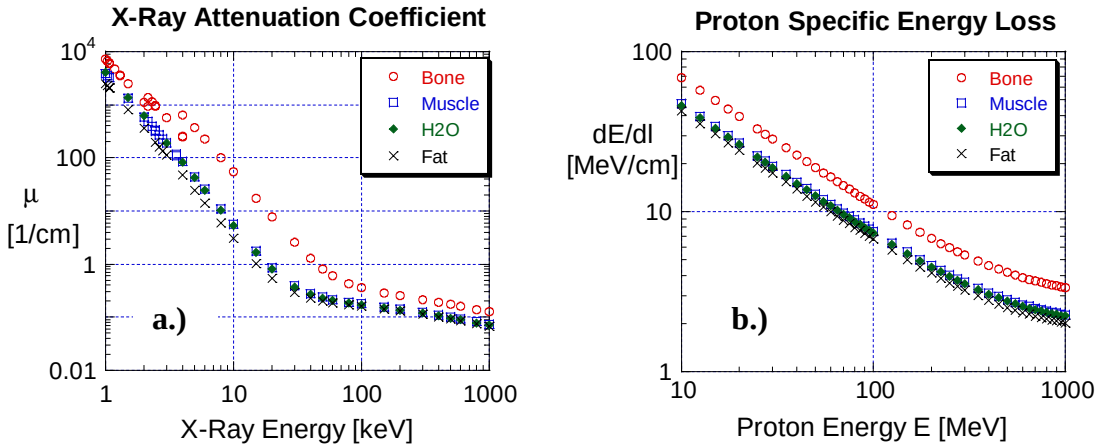

Fig. 1. (a) X-Ray attenuation coefficient and (b) proton specific energy loss as a function of energy for bone, muscle, water and fat [3]. The large contrast for bone in X-rays is due to factor 10 times larger attenuation coefficient with respect to water, while the difference between different tissue and water is relatively small both in X-rays and protons. The energy dependence of the specific energy loss can be employed to measure the particle energy.

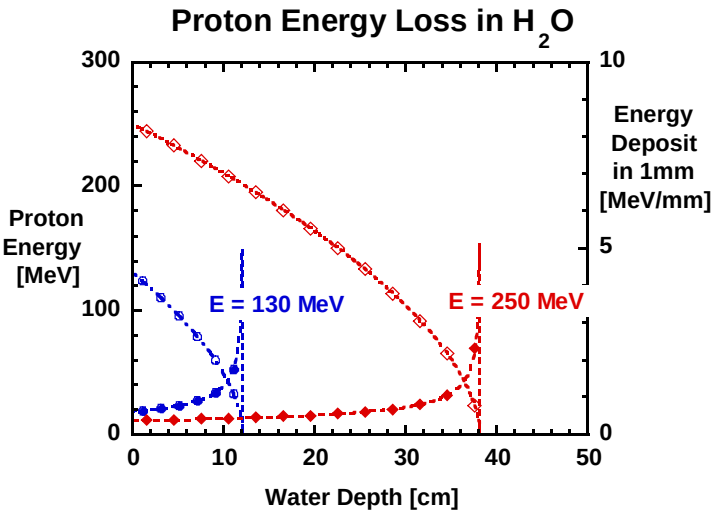

Fig. 2. Proton energy loss in water as a function of penetration depth for two incident proton energies [3]. The left hand scale indicates the energy of the protons (open symbols), and the right hand scale the energy deposited in 1 mm water (closed symbols). The energy deposit is characterized by an entrance plateau, and the so-called Bragg peak at the end of the range, which is used in proton beam treatment to deliver maximum dose to the tumor. Beyond the well-defined range the intensity exhibits a rapid distal fall-off. In Proton CT, the energy loss of protons in the plateau would be used, which will minimize the dose to the patient.

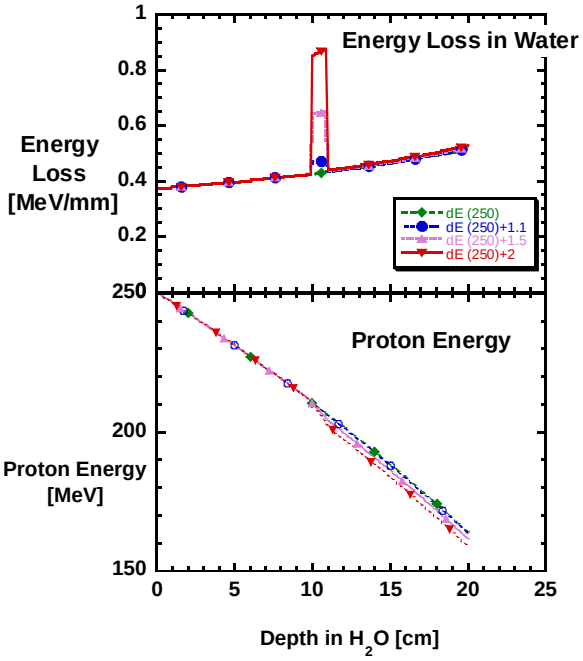

Fig. 3. Proton energy loss in water as a function of penetration depth for 250 MeV protons, with a 1cm long inclusion of varying density at a depth of 10cm. The densities chosen are ρ = 1, 1.1, 1.5, 2 g/cm2. a) Energy loss in 1 mm. b) Proton energy. Although the difference in energy loss is substantial locally, the effect of changed density is barely visible at a depth of 20 cm (see Table 1). A density of ρ = 1.5 corresponds to bone, and of ρ = 1.1 to different tissue.

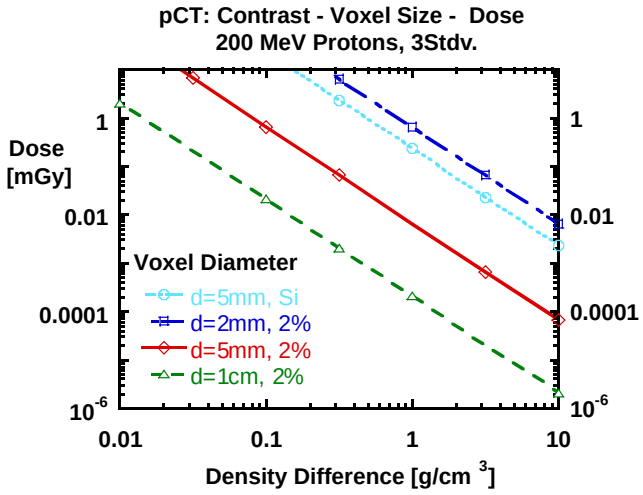

Fig. 4. Dose – Contrast relationship for 200 MeV protons for different voxel sizes d. The lines indicated by 2% assume a calorimeter with 2% resolution, and the one indicated by Si the energy resolution achievable with silicon strip detectors (20%).

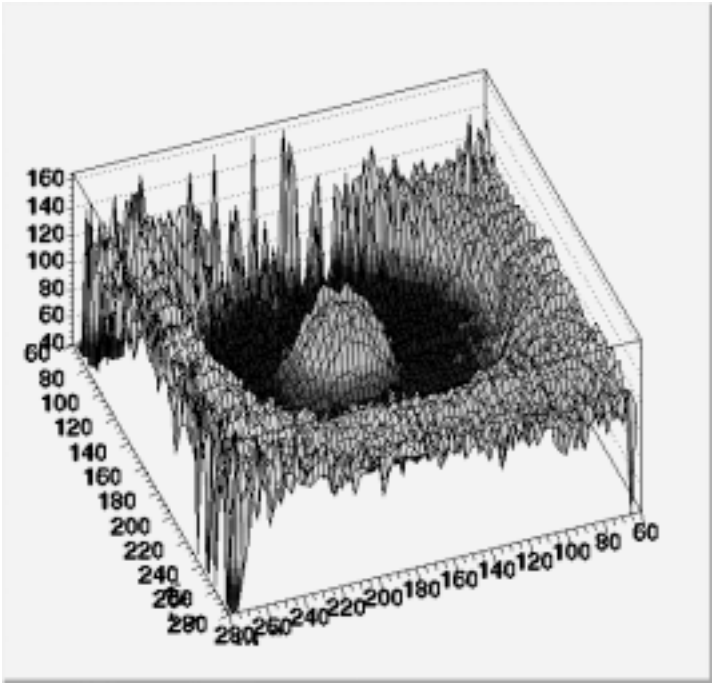

Fig. 5. Spatial distribution of the average energy of protons with single-strip resolution at the level of the upstream SSD module [7]. The increased energy loss in the pipe is clearly visible.

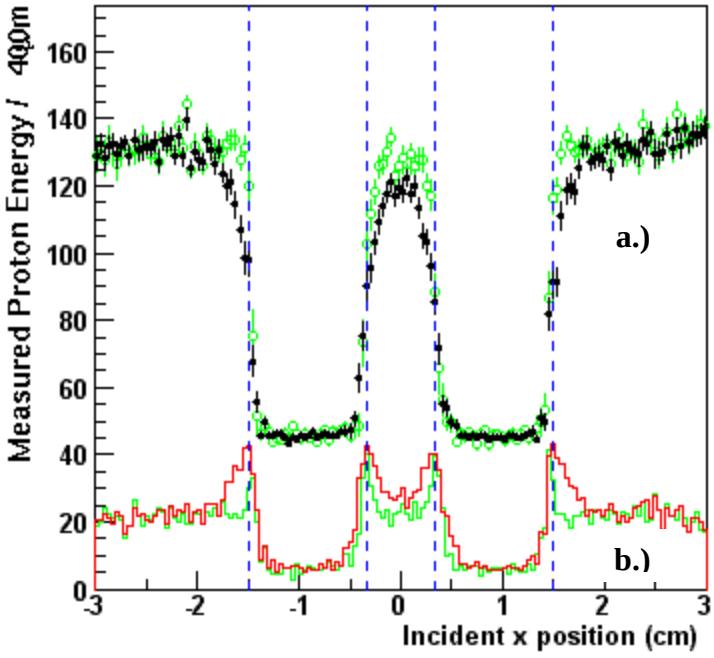

.

Fig. 6a (upper half of illustration). Monte Carlo simulation of the average energy profile of the first SSD module in a 400 μm wide slice through the center of the object as indicated in Fig. 5. The dashed vertical lines indicate the relative position of the object with respect to the SSD plane.

Fig. 6b (lower half). RMS deviation of the proton energy. Note the increase in the RMS at the interfaces between object and air.

The closed symbols and the red histogram are for all particles, and the open circles and the green histogram are for protons within the angular cut of 0.025. The improvement in image sharpness is seen in the more vertical interfaces, filling in the hole, and the reduction of the width of the region with increased energy RMS at the pipe-air interface [6].